

Article

Non-Conventional Hybrid Microporous Layers for Enhanced Performance and Durability of PEM Fuel Cells

Saverio Latorrata ¹, Marco Mariani ², Andrea Basso Peressut ^{1,*}, Riccardo Balzarotti ³
and Giovanni Dotelli ¹

¹ Department of Chemistry, Materials and Chemical Engineering “Giulio Natta”, Politecnico di Milano, Piazza Leonardo da Vinci 32, 20133 Milano, Italy

² Department of Mechanical Engineering, Politecnico di Milano, Via La Masa 1, 20156 Milano, Italy

³ Mechanical Engineering and Materials Technology Institute (MEMTi),

University of Applied Sciences (SUPSI-DTI), Via la Santa 1, 6962 Lugano, Switzerland

* Correspondence: andreastefano.basso@polimi.it

Abstract: In this work, novel microporous layers (MPLs) were developed based on fluorinated ethylene propylene (FEP), as a hydrophobic agent, and carboxymethylcellulose (CMC), as a wettability modulator and rheology controller for the inks, which were deposited onto pre-hydrophobized macroporous gas diffusion layers (GDLs). Higher CMC amounts led to higher dynamic viscosities of the inks, which induced the formation of a more compact and less cracked MPL surface. Different concentrations of CMC were tested and the experimental measurements showed a threshold limit pointing out an optimal composition that positively affected the electrochemical performances at medium-low relative humidity (RH), which is important to mitigate the need of saturating inlet gases. Durability of the best performing samples was assessed by means of an ad hoc developed accelerated stress test (AST) and compared to one of the conventional FEP-based GDMs. It was found that a lower decrement of both the output power density and the overall cell efficiency can be obtained upon the ASTs with the novel samples.

Keywords: PEM fuel cells; gas diffusion layer; MPL; coating; hydrophobicity; durability; accelerated stress tests; output power density; cell efficiency



Citation: Latorrata, S.; Mariani, M.; Basso Peressut, A.; Balzarotti, R.; Dotelli, G. Non-Conventional Hybrid Microporous Layers for Enhanced Performance and Durability of PEM Fuel Cells. *Physchem* **2023**, *3*, 78–91. <https://doi.org/10.3390/physchem3010007>

Academic Editor: Jacinto Sá

Received: 19 November 2022

Revised: 26 December 2022

Accepted: 18 January 2023

Published: 22 January 2023



Copyright: © 2023 by the authors. Licensee MDPI, Basel, Switzerland. This article is an open access article distributed under the terms and conditions of the Creative Commons Attribution (CC BY) license (<https://creativecommons.org/licenses/by/4.0/>).

1. Introduction

Polymer electrolyte membrane fuel cells (PEMFCs) have been attracting widespread attention as alternative energy generators thanks to their remarkable efficiency, limited operating temperatures with respect to other systems (e.g., solid oxide fuel cells) and lower emissions compared to fossil fuel-based systems, especially when fed with green hydrogen. Together with the growing range of electrochemical energy conversion and storage solutions, PEMFCs could be operated as on-demand electricity generators exploiting stored green hydrogen, produced during peak production hours from renewables, thus closing the gap among excess load production and demand curves [1]. Several technological efforts are continuously spent to develop advanced materials for enhancing the performance of such devices in terms of output power density and overall efficiency [2–6]. Various studies have proved that the water management of PEMFCs is crucial for a proper and effective operation, particularly for the cathodic compartment [7–9], and the gas diffusion medium (GDM) is the most relevant component in this regard. It is inserted between the flow field of the bipolar plate and the electrode, and it is formed by a macroporous carbon-fiber-based substrate (gas diffusion layer, GDL) and a microporous layer (MPL). It must be hydrophobic as its main function is the removal of liquid water from the catalyst layer and its transport toward the flow channels induced by the capillary suction generated by its microporosity. However, liquid water is not only produced at the cathode by the oxygen reduction reaction, but it is also fed by external saturators to keep the polymer electrolyte hydrated,

which is essential for having a suitable proton conductivity. An excess of such water, often referred to as flooding, could accumulate in the porous components and in the channels of the fuel cell and could cause diffusion limitations with a consequent increase in the mass transfer resistances and of the related concentration polarization [10–13]. Therefore, an appropriate balance between the water needed for the membrane hydration and the one produced by the electrochemical process is necessary, which is accomplished by the GDLs and MPLs [14].

GDLs are macroporous carbon-fiber clothes or papers with variable thickness in the range 100–400 μm ; they are responsible of a uniform diffusion of the reactants to the active area and of the electrical contact between the bipolar plate and the electrode [3]. MPLs are deposited onto the GDL surface and are generally made from dispersions containing carbon black and fluoro-polymeric binders (usually polytetrafluoroethylene (PTFE), fluorinated ethylene propylene (FEP), polyvinyl-fluoride (PVDF) or perfluoropolyether (PFPE)) [15–19]; they are thinner hydrophobic layers (usually 10–50 μm) with several micropores that improve water removal and the gas reagents' uniform distribution. Such a coating also improves the smoothness of the GDM surface, allowing a better contact with the catalytic layer and a consequent higher electrical conductivity [20,21]. Moreover, MPLs are also able to reduce mass transport limitations and to improve performances, especially in the high current density region [22]. On the other hand, excessive dehydration would be equally detrimental and the performance of the fuel cell would decrease because the ionic conductivity of the proton membrane is strongly dependent on the water content [23]. In order to keep the electrolyte hydrated even in conditions of low humidity, hydrophilic species can be properly added to the inks for the MPLs' production, still preserving the overall hydrophobic behavior of the whole GDM, which is needed to avoid the flooding phenomenon [24,25].

The MPLs are often deposited onto the GDLs by means of the blade-coating technique. Such a technique requires the use of pseudo-plastic, shear-thinning fluids, which influence the effect of the MPL formulation on the fuel cell electrical performance [25]. During the preparation of the inks, undesired instability phenomena may take place because of possible separations of the carbon powders in the aqueous solution. In some past applications, carboxymethylcellulose (CMC) has been employed as a stability and rheology controller thanks to its capability to prevent the coalescence of solid nanoparticles, thus impeding the negative consequences of flocculation and leading to stable dispersions (i.e., with constant values of dynamic viscosity) for several days [26]. At the same time, CMC allowed to easily disperse carbon-based powders in aqueous fluids, attaining a shear-thinning behavior of the inks, which is suitable for the blade-coating technique, and to improve the performance of the fuel cell assembled with the CMC-containing single layer MPLs in terms of ohmic resistances and output power density at low cathodic relative humidity [26,27].

In this paper, CMC and fluorinated ethylene propylene (FEP) were used on the basis of previous works that have highlighted their beneficial effects on inks formulation and water management of the running fuel cell, respectively. Indeed, FEP has proved to be an effective alternative to conventionally used PTFE as both a binder and hydrophobic agent for the GDLs and MPLs, since it allowed to reduce the maximum temperature of the thermal treatment of about 25% with respect to the one needed with the PTFE-based MPLs, and to enhance water management at high current density thanks to a higher hydrophobicity [25,28].

The effect of CMC on the rheological properties and electrical performances of a single PEMFC is reported and compared with the behavior of the CMC-free samples. Double MPLs were developed aiming to achieve the enhancement of PEMFC performance under low humidification at the cathode; a first FEP-based MPL was deposited onto the pre-hydrophobized GDL, then a thinner CMC-containing layer was added, which was supposed to be effective to preserve the membrane's water content [29,30], and this should help to reduce the stringent need of using saturated inlet reactants. Indeed, the usually employed electrolytic membrane is Nafion, a perfluorosulfonic ionomer with

lateral sulfonic acid groups releasing protons under proper hydration, thus enabling charge transportation across the electrolyte [31].

2. Materials and Methods

Commercial carbon cloth GDLs (SCCG 5N, SAATI Group, Appiano Gentile, Italy) were used as macroporous substrates for the MPL deposition. The GDLs were soaked in an aqueous suspension of 12 wt.% fluorinated ethylene propylene (FEP, Chemours Italy S.r.l., Monza, Italy) for 20 min in order to be made hydrophobic. Subsequently, they were dried at room temperature and heated in air for 30 min up to 270 °C to melt the polymer, to make it fibrous and to allow it acting as a binder too.

Contextually, carbon-based dispersions, more often named inks, were prepared as a basis for the MPL coating. Specifically, Vulcan carbon black XC72R and multiwall carbon nanotubes (relative ratio 90/10 wt./wt.), supplied by Cabot, were mixed with appropriate amounts of a commercial 55 wt.% FEP suspension, water and isopropyl alcohol (IPA, Sigma Aldrich Italia S.r.l., Milan, Italy). The mixture was stirred with an UltraTurrax T25 homogenizer (Ika Werke, GmbH, Staufen, Germany) for 10 min at 8000 rpm; subsequently, four different amounts of CMC (Lamberti S.p.A., Albizzate, Italy) (from 0.25 wt.% up to 2 wt.% with respect to the water content) were added and the resulting mixture was stirred again at the same rate. The slurry without CMC was prepared using the same procedure described above with a composition studied in a previous paper [32]. For this reason, hereafter it will be referred to as “standard ink” in the text. In Table 1, the relative amounts of the ink components are reported.

Table 1. Inks composition in terms of relative amounts of the employed components.

Ink	C-Phase ¹ /H ₂ O [w/w]	FEP/C-Phase [w/w]	IPA/C-Phase [w/w]	CMC/H ₂ O [w/w]
no CMC	0.13	0.12	5.6	0
CMC-0.25	0.13	0.12	5.6	0.25
CMC-0.5	0.13	0.12	5.6	0.5
CMC-1	0.13	0.12	5.6	1
CMC-2	0.13	0.12	5.6	2

¹: C-phase represents the total amount of carbonaceous components, i.e., carbon black and carbon nanotubes.

The prepared standard ink was deposited onto the GDL substrate via the blade-coating technique, using lab-scale commercial equipment (K Control Coater, RK Print Coat Instruments, Litlington, UK). A linear velocity of 1.54 cm/s and a 40 µm gap between blade and substrate (i.e., the desired thickness of the wet coating) were adopted. The coated samples were calcined up to 270 °C for 30 min.

For fabricating double MPLs, firstly a 30 µm layer of standard ink was deposited onto the GDL and the resulting MPL was heated at 270 °C for 30 min; subsequently, each CMC-containing ink was deposited (with a 10 µm gap) onto the standard layers and heat-treated in the same way. Figure 1 summarizes the steps of the preparation procedure of the standard and CMC-based GDLs.

A Cambridge Stereoscan 360 scanning electron microscope (SEM) was used for the morphological analyses of the MPL surface. Accelerating voltage of 20 kV, current probe of 200 pA and chamber pressure of 10⁻⁵ Pa were adopted. The homogeneity of the MPL surface and the coverage degree of the substrates were evaluated by acquiring images at 40× magnification. In order to make the surfaces of the MPLs fully conductive, a gold nanolayer was sputtered on them.

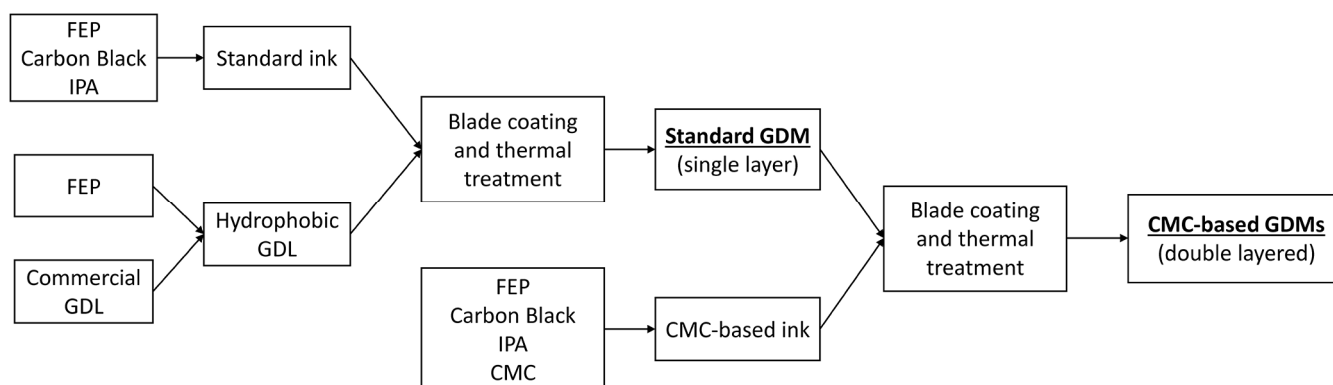


Figure 1. Visual flow chart reproducing the production process of standard and CMC-based GDMs.

In order to assess the hydrophobicity of the GDMs, static contact angles of the samples were measured according to the sessile drop technique with an OCA 20 system (DataPhysics instruments, Filderstadt, Germany) equipped with a CCD video-camera (resolution of 752×582 pixels, 50 frames s^{-1}). Values reported in this paper for each sample are the result of the average of ten measurements.

The pores diameter, pore size distribution and pore volume/porosity of the prepared GDMs after thermal treatment were measured by the mercury intrusion technique using a Porosimeter 2000 Series instrument (2000 bar maximum pressure) by Carlo Erba (Cornaredo, Italy). The pore size distributions were calculated by applying the Washburn equation.

GDMs were assembled in a 25 cm^2 lab-scale fuel cell and tested electrochemically with a bench test station by Fuel Cell Technologies. A commercial membrane electrode assembly (Baltic Fuel Cells GmbH, Schwerin, Germany) was employed for the tests: it consisted of a Nafion 212 electrolytic layer ($50.8 \mu\text{m}$ thick) and coated electrodes with a platinum loading of 0.2 mg cm^{-2} at the anode and 0.4 mg cm^{-2} at the cathode. Polarization and power density curves were collected imposing current (from OCV configuration, i.e., null current, to 1.32 A cm^{-2} , $0.09 \text{ A cm}^{-2}/\text{step}$) with the RBL 488 50-150-800 electronic load by TDI Power (Hackettstown, NJ, USA). Hydrogen and air flow rates were controlled by calibrated flowmeters (Smart Mass flowmeters by Brooks Instrument, Hatfield, PA, USA) and set at 0.25 and 1 NL min^{-1} , respectively; relative humidity (RH) was controlled by external humidifiers. Experiments were carried out at two different cell temperatures ($60 \text{ }^\circ\text{C}$ and $80 \text{ }^\circ\text{C}$); one humidity condition was employed for the hydrogen flow ($80\% \text{ RH}$), while two different values (60 and $100\% \text{ RH}$) were adopted for the air feeding in order to evaluate the effect of low and high humidity on the cathodic water management.

Electrochemical impedance spectroscopy (EIS) was carried out using a frequency response analyzer (FRA, Solartron 1260, Farnborough, United Kingdom). The spectra were obtained at the same current density values of the polarization measurements, in galvanostatic mode, over a frequency range from 0.5 to 10 kHz (10 points per decade). All the experimental data were fitted using the Zview[®] software (Solartron) and ohmic, activation polarization and diffusion resistances were extracted from electric circuit modeling [33]. The equivalent electrical circuit employed for modeling internal losses (Figure S1, Supplementary Materials) consisted of a first resistance (ohmic losses) in series with two parallel circuits: the former to model charge transfer resistance by quantification of the activation polarization; the latter to model mass transfer resistance from concentration polarization. Constant phase elements (CPE) were employed instead of pure capacitances as circuit elements, to better reproduce the porosity-related behavior of the components [33].

An evaluation of durability was also performed on the best performing double-layer GDM. First, a preliminary test was executed by keeping the fuel cell at constant current density: 0.5 A cm^{-2} was selected as a representative value for real applications [28] and kept fixed for 1000 h at $60 \text{ }^\circ\text{C}$ and $\text{RH } 80\text{--}60\%$. Moreover, an ex situ mechanical acceler-

ated stress test (AST) was also designed on the same samples in order to have a faster assessment of the durability of the prepared components in terms of mechanical resistance without performing continuous tests for thousands of hours, which is a common practice also for electrochemical ASTs evaluating degradation of different fuel cell components, such as electrodes or membrane [34,35]. Indeed, it has been demonstrated that the most detrimental degradation mechanism for GDMs is the mechanical one, which is due to both the continuous flow of the gaseous streams and the presence of water causing the detachment of the MPL surface carbon [28]. As reported in previous works [36,37], in an ad hoc experiment, the GDMs were assembled in a dummy cell, featuring a Teflon inert separator without catalysts in order to prevent chemical stresses on the samples. For the same reason, hydrogen was not used as anodic feeding and only air was supplied continuously for 1000 h to each compartment of the cell with a twofold flow rate (0.5 NL min^{-1} at the anode and 2 NL min^{-1} at the cathode) compared to the one employed for standard polarization tests to promote mechanical degradation. After ASTs, electrochemical tests were carried out again in the same operating conditions as constant current experiments in order to evaluate the change in performance induced by degradation.

3. Results

3.1. Morphology

The SEM images of the double-layer (DL) coatings' surfaces upon thermal treatment are reported in Figure 2.

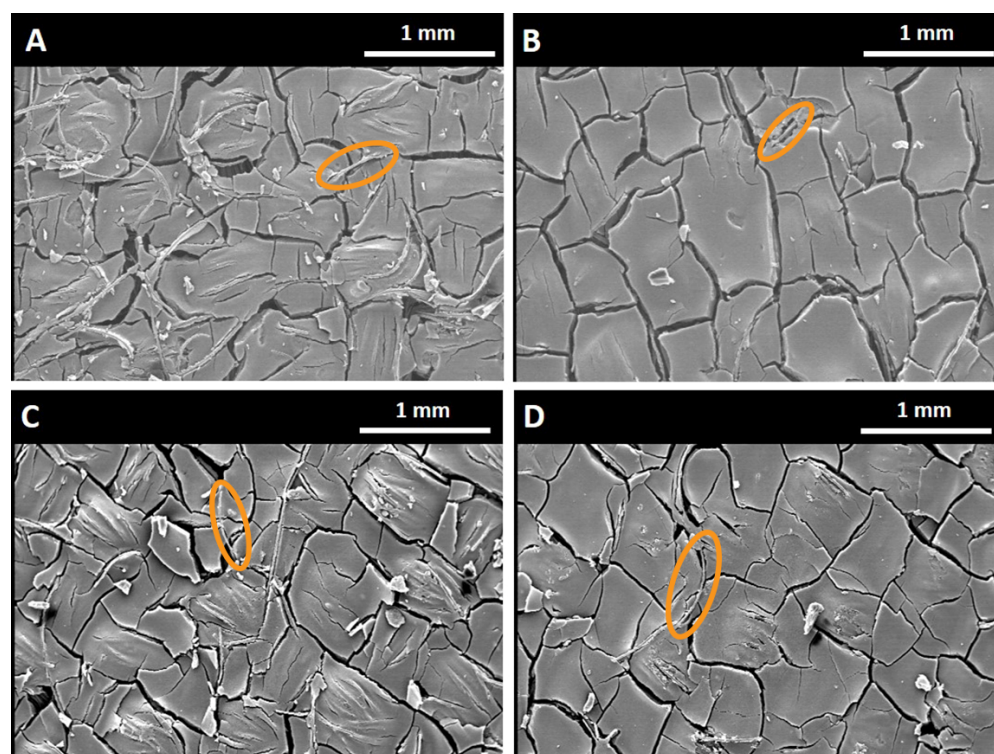


Figure 2. SEM images of the CMC-containing MPLs: (A) CMC-0.25 DL, (B) CMC-0.5 DL, (C) CMC-1 DL, (D) CMC-2 DL. Orange ellipses highlight examples of partially exposed fibers.

All the coatings show very similar surfaces among them and to that of the reference FEP-based MPL developed in a previous work of ours [28] (Figure S2, Supplementary Materials), thus excluding a relevant effect of the CMC content on the MPL surface morphology. A good coverage of the substrates has been achieved, indeed because each sample weft and warp of the underlying clothes is not evident or only slightly visible with some uneven fibers identifiable, as highlighted in Figure 2. Cracks are always present due to the evaporation of the inks' solvents during thermal treatment. However, it seems that smaller

and less pronounced cracks were formed for the CMC-containing MPLs: by means of the ImageJ processing program, it was found that the cracks represent 17% of the standard MPL surface while 9–12% of the CMC-based MPLs. Such behavior may be ascribed to the effect of CMC as a rheology modulator in increasing the viscosity of the inks: as a matter of fact, more viscous slurries might feature a reduced coalescence tendency prior to heat-treatment, leading to more compact coatings (rheological flow curves in Figure S3, Supplementary Materials). On the other hand, the viscosity seems to have no drastic effect on the thickness of the final layers, as shown in Table 2, which excludes the detrimental effect on the oxygen transport resistance from the addition of CMC [38]. Indeed, a quasi-constant value (average in the range 49–52 μm) was obtained since only the wet layer (i.e., immediately after the blade-coating has been applied) is directly linked to the slurry viscosity [26], whereas the final thickness depends on the total solid content that in turn keeps practically constant upon the liquid’s evaporation. In the same table, the average static contact angle and average pore diameter are reported as well, the latter having been obtained from the porosimetry measurements (Figure 3).

Table 2. Average thickness of the MPLs, static contact angle (MPL side), average pore diameter of the GDMs and dynamic viscosity (at shear rate of 100 s⁻¹) of the inks used to deposit the MPLs.

Sample	Average Thickness [μm]	Static Contact Angle [°]	Average Pore Diameter [nm]	Dynamic Viscosity at 100 s ⁻¹ [Pa s]
no CMC ¹	50	158 ± 3	45	0.176
CMC-0.25 DL	51	144 ± 8	40	0.179
CMC-0.5 DL	52	137 ± 6	44	0.359
CMC-1 DL	49	134 ± 5	49	0.522
CMC-2 DL	51	129 ± 3	72	0.975

¹ reference [28].

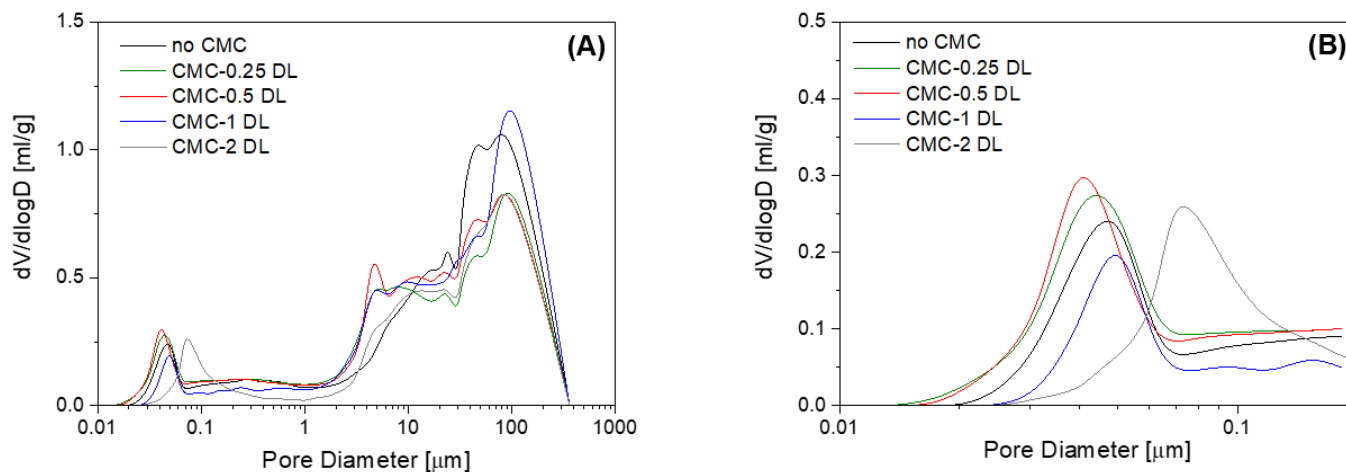


Figure 3. Pore size distribution obtained via the mercury intrusion porosimetry technique (A), enlargement of the microporous region (B).

Despite the hydrophilic feature of CMC, the double MPLs were able to keep a satisfying hydrophobicity, which may result in an effective water management for all the samples within the cell during running. However, the addition of CMC—which is supposed to leave some residues after the thermal treatment (see TGA in Figure S4)—causes a progressive decrease in the average static contact angle, even though such behavior is not dramatic. In addition to the hydrophilic nature of CMC, this reduction may be partially correlated to the increase in the average pore diameter: the capillary repulsion induced by the hydrophobic porosity of the MPL surface is inversely proportional to the radius of the capillary itself, thus affecting the shape of the deposited droplets [39].

In addition, all samples show a deviation from the average values, which could be related to the heterogeneity and to the cracks originated after the thermal treatments [40,41].

The pores size distribution of the five GDMs was measured, and the results are shown in Figure 3.

It seems that pore volume is not sharply dependent on the composition and deposition methodology. While the macropores (average pore diameter higher than 7 μm) are mostly related to the fixed GDLs and to the gas transport across them from the flow field, the microporous region (average pore diameter lower than 0.07 μm) is the most crucial one for a proper water capillary condensation, thus for an effective removal [20]. It appears to be very similar for all samples in terms of the extent of the micropores and of the average pores diameter, which is also comparable with values obtained in a previous work for the standard PTFE-based MPL, showing an average pore diameter around 0.05 μm [42]. Only the CMC-2 DL sample, containing the largest amount of CMC, showed a slight shift of the microporous distribution toward larger values (more clearly observable in the distribution magnification in Figure 3B), leading to an average pore diameter of about 0.072 μm instead of 0.04–0.05 μm for the other samples. This could be ascribed to a larger extent of water removal during the thermal treatment in the case of a higher CMC content or to a larger amount of partially decomposed CMC that would have left bigger pores, given that the molecule is also used as a pore-former [43].

3.2. Electrochemical Characterization

The polarization and power density curves obtained at the exploited operating conditions for the fuel cells assembled with the different double MPLs are displayed in Figure 4.

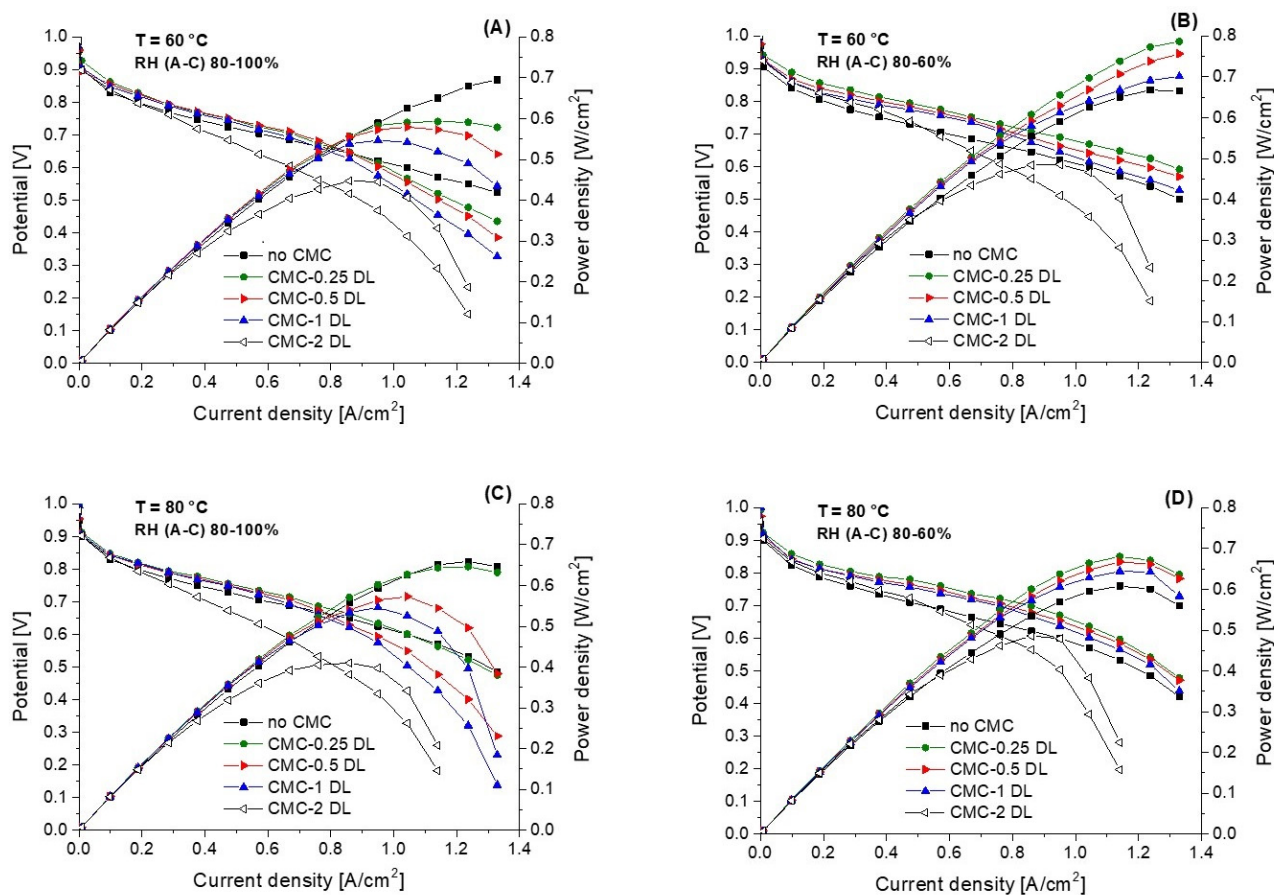


Figure 4. Polarization curves obtained at (A) 60 °C and RH (A-C) 80–100%, (B) 60 °C and RH (A-C) 80–60%, (C) 80 °C and RH (A-C) 80–100%, (D) 80 °C and RH (A-C) 80–60%.

At certain operating conditions, fuel cells assembled with the CMC-containing layers, except for the sample with the highest content of CMC (CMC-2 DL), showed an improvement in electrical performances. In detail, at low cathodic RH (60%, Figure 4B,D), the double-layered samples resulted in higher power densities, whereas, at high RH (Figure 4A,C), they showed comparable results to the CMC-free based fuel cell at the current density values lower than 0.7 A cm^{-2} and a worsening of performance at the higher current densities. Thus, the presence of a CMC-containing second layer seems effective in improving electrical performances at low RH. Indeed, the presence of CMC, acting as a sort of water reservoir, should prevent the membrane's dehydration. This could provide an increase in the membrane's conductivity with respect to the case in which it is dehydrated or a CMC-free MPL is used, thus reducing the overall cell resistance and resulting in a higher power density at low RH. Moreover, the co-presence of the CMC-free layer, just beneath the CMC-containing one, and the preservation of the micropore fraction efficiently eliminate excess water. This points out that considerable advantages may be obtained in the double-layered samples when both effects are coupled [44,45].

At high humidity, the water adsorption due to CMC likely limited the reaction rate and resulted in worse electrical performances and in sharp voltage drops in the region where more water is generated, i.e., at high current densities.

Considering the above results, it seems that, for these materials, the operating temperature does not have a pronounced effect on performances, while the RH is a crucial parameter. Accordingly, the CMC-containing GDMs should be selected with proper operating conditions to obtain the most satisfying results.

The worst performances were found with the double-layer MPLs containing 2 wt.% CMC, which did not give any advantages at any operating condition. This likely suggests a certain threshold CMC concentration that must be avoided in order to prevent critical diffusive issues.

From experimental impedance spectra, internal resistances, i.e., different polarization contributions, were extracted. Figures 5 and 6 report, respectively, the ohmic resistance and the mass transfer (or diffusion) resistance as a function of the current density, as these are the parameters mostly influenced by the nature and effectiveness of the GDM.

From Figure 5, it is evident that the samples with CMC are able to reduce definitely the ohmic resistance (R_{Ω}) at any operating condition compared to the free-CMC sample [46]. Indeed, the presence of the hydrophilic CMC acting as water reservoir is effective in ensuring a better hydration of the electrolyte and the catalytic interface, and therefore a lower overall ohmic resistance. However, no sensible effect of the CMC amount is observable, likely due to the very close thicknesses of the layers of these samples. Moreover, at any condition, the ohmic resistance keeps quasi-constant upon increasing the current density. Finally, as expected, an increase in the RH, at a fixed temperature, leads to a reduction in R_{Ω} , both at $60 \text{ }^{\circ}\text{C}$ and at $80 \text{ }^{\circ}\text{C}$. Similarly, when the RH is kept constant, an increase in temperature causes a decrease in R_{Ω} , but in some cases more limited.

Figure 6 shows the trend of the diffusion resistance, R_d , as a function of the current density. An expected increase of R_d is manifest due to increasing water production, which hinders the transport of reactants toward the electrode. The CMC-based MPLs show a similar qualitative trend as the standard MPLs, but, once more, the highest content of CMC (CMC-2 DL) confirms being detrimental at high current densities. However, for a lower content of CMC a better performance is observed, especially at low RH; indeed, both at $60 \text{ }^{\circ}\text{C}$ and at $80 \text{ }^{\circ}\text{C}$ (Figure 6B,D) the R_d parameters obtained with the double MPLs, except for CMC-2 DL, are very similar to those obtained with the standard MPL (no CMC). This confirms that, at low RH, the double MPLs guarantee performances and water management comparable with those of the standard MPL; this behavior, coupled with the measured lower ohmic resistances, results in overall better performances of the double-layered samples, as already demonstrated by the polarization curves (Figure 4).

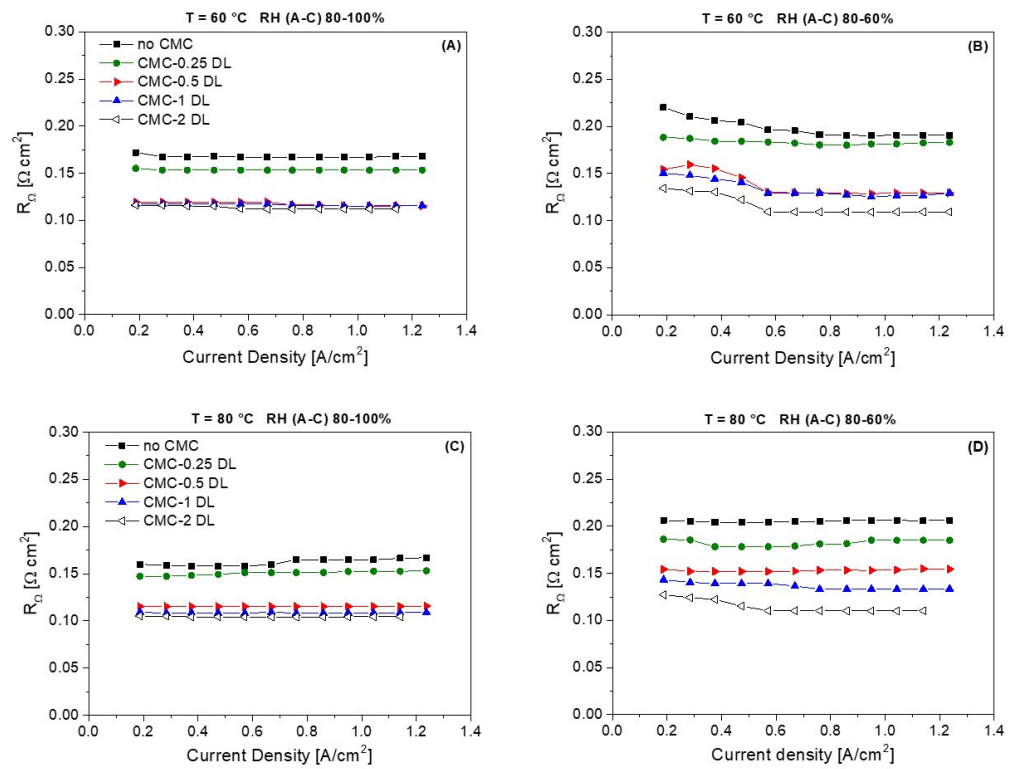


Figure 5. Ohmic resistance as a function of current density at (A) 60 °C and RH (A-C) 80–100%, (B) 60 °C and RH (A-C) 80–60%, (C) 80 °C and RH (A-C) 80–100%, (D) 80 °C and RH (A-C) 80–60%.

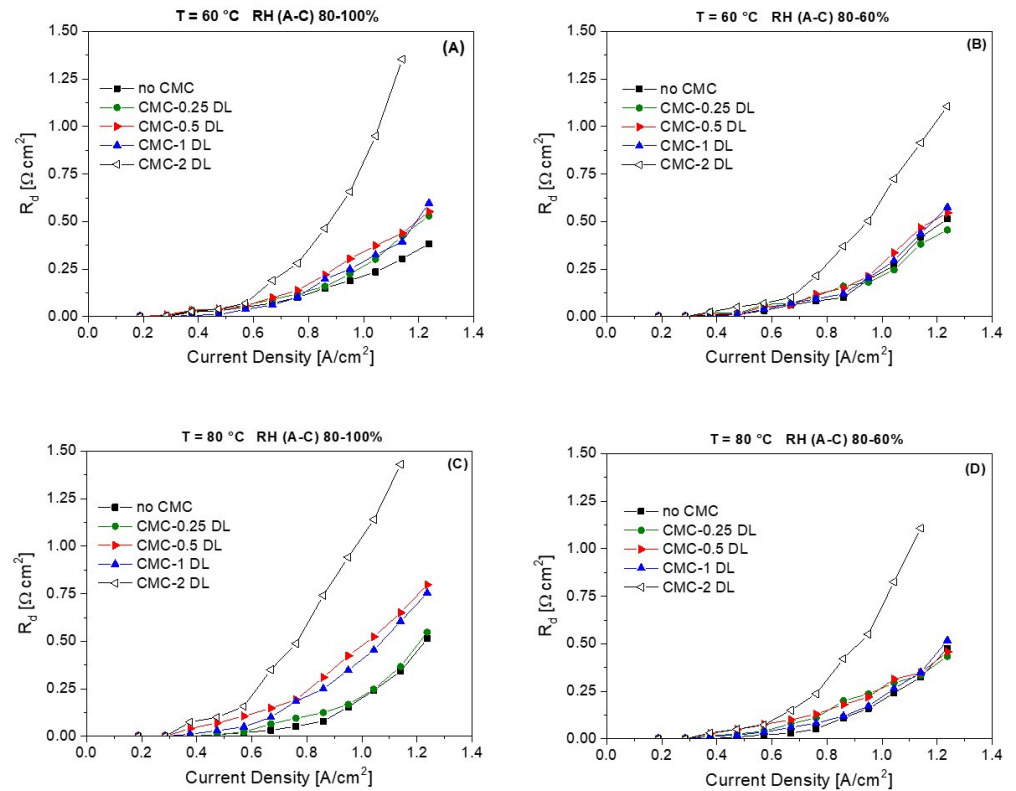


Figure 6. Diffusion resistance as a function of current density at (A) 60 °C and RH (A-C) 80–100%, (B) 60 °C and RH (A-C) 80–60%, (C) 80 °C and RH (A-C) 80–100%, (D) 80 °C and RH (A-C) 80–60%.

3.3. Durability

Figure 7 shows the polarization curves obtained after performing 1000 h of the AST and constant current durability tests for the fuel cells assembled with the best performing CMC-based samples (CMC-0.25 DL). Concerning the constant current experiments, only a slight voltage drop occurred at a high current density compared to the performance of the fresh sample (i.e., the one tested without any aging). This may be due to the accumulation of water over time in the cathode serpentine, but real negative effects due to the GDMs are not visible. On the contrary, the sample subjected to the AST exhibited a clear performance loss in the medium-high current density region (i.e., $>0.9 \text{ A cm}^{-2}$); however, it is also evident that the efficiency in the ohmic region could be regarded still acceptable in real applications (variation of 2.9% at 0.5 A cm^{-2} , reported in Table 3). Indeed, in the linear part, the polarization curve obtained upon the AST is only slightly lower than the fresh and constant current tested samples. The observed decrement in the maximum output power is about 17%, but is lower than that calculated for non-containing CMC (21.8%) [32].

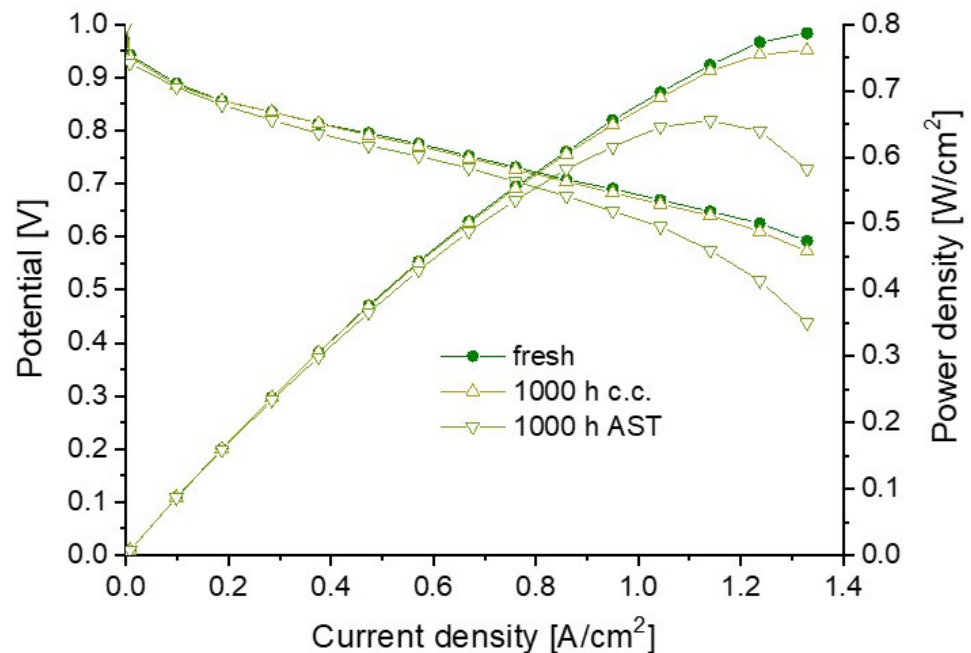


Figure 7. Polarization and power density curves obtained with the CMC-0.25 DL samples upon constant current tests and AST, compared with the fresh sample.

Table 3. Variation of the maximum output power density and global cell efficiency upon ASTs.

Sample	ΔP_{AST} [%]	$\Delta \eta_{gc}$ [%]
no CMC ¹	21.8	4.7
CMC-0.25 DL	16.8	2.9

¹ reference [32].

The ohmic resistance keeps stable upon performing constant current tests, thus confirming no sensible effects of such experiments on material degradation and durability of the whole fuel cell (Figure 8A). For the AST-treated GDM, a negligible raise of the ohmic resistance is observed likely due to the defects introduced within the structure and on its surface, reducing the contact uniformity with the catalyst layer. A different behavior can be observed considering the trend of diffusion resistance (Figure 8B): samples subjected to the AST exhibited a dramatic worsening of the water management (i.e., an evident increase in R_d) starting from the medium current density values, as previously noticed with the

polarization curves. In this case, also samples tested with constant current experiments have shown a higher diffusion resistance compared to fresh GDMs, but only at very high current density values, likely due to the accumulation of water in the porosity of the related components, as pointed out in the polarization tests. It is safe to say that the GDMs' performances are stable as long as major physical degradation of the MPLs does not occur.

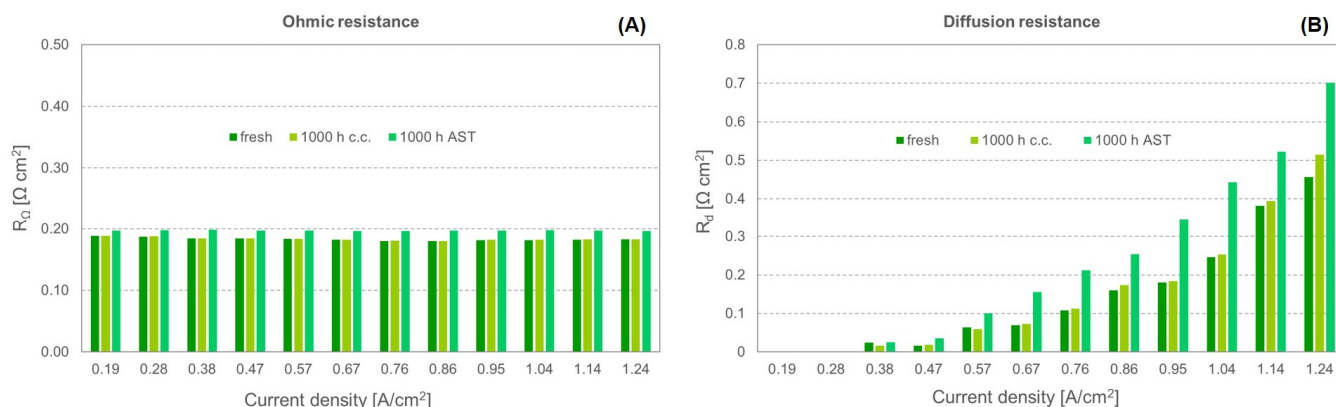


Figure 8. Ohmic (A) and mass transfer resistances (B) as a function of the current density upon constant current tests and AST, compared with the fresh sample.

4. Conclusions

An organic hydrophilic molecule such as CMC has been employed to manage and control the overall wettability of FEP-based gas diffusion media for PEM fuel cells. Inks with different CMC concentrations were prepared and deposited via blade-coating technique on hydrophobic MPLs and in turn applied onto the FEP pre-treated GDLs. Therefore, the double-layer MPLs were obtained, being formed by a first conventional layer and a second CMC-based one.

All the developed MPL surfaces are quite homogeneous, even though some cracks are always evident because of the thermal treatment needed to sinter and consolidate the coating. The double MPLs showed a lower content of cracks on increasing the CMC amount, whereas similar thicknesses were obtained.

The hydrophobic samples were attained but the presence of residual CMC decreased slightly the static contact angle. The CMC effect on the running fuel cell strongly depends on the selected operating conditions. Except for the highest content of CMC employed (2 wt.%), the double MPLs improved electrical performances at low cathodic RH and were able to better manage water, even at high current densities. At high cathodic RH, CMC resulted detrimental as it led to excessive water retention at high current densities.

The CMC-based samples were also able to reduce ohmic resistances at each operating condition because of the CMC capability of keeping the electrolyte hydrated, thus increasing the proton conductivity.

The best performing CMC-based sample was subjected to accelerated stress tests (ASTs) and it was found that such GDM is able to reduce the change in the maximum power density and overall global cell efficiency compared to the CMC-free samples, which could enhance the overall durability.

Supplementary Materials: The following supporting information can be downloaded at: <https://www.mdpi.com/article/10.3390/physchem3010007/s1>, Figure S1: Equivalent circuit used for modeling impedance spectra and example of three spectra collected at (A) low (0.17 A/cm²), (B) medium (0.43 A/cm²) and (C) high current density (0.79 A/cm²). Sample: CMC-0.25 DL, operating condition: 80 °C and RH (A-C) 80–60%; Figure S2: SEM picture of a single layer MPL without CMC; Figure S3: Rheological flow curves of the inks containing and non-containing CMC; Figure S4: TGA of CMC.

Author Contributions: Conceptualization, S.L. and R.B.; methodology, S.L. and R.B.; validation, S.L., M.M. and A.B.P.; formal analysis, S.L., M.M. and R.B.; investigation, S.L., M.M. and R.B.; resources, G.D.; data curation, S.L., M.M. and A.B.P.; writing—original draft preparation, S.L. and M.M.; writing—review and editing, A.B.P. and R.B.; visualization, S.L. and M.M.; supervision, G.D. All authors have read and agreed to the published version of the manuscript.

Funding: This research received no external funding.

Data Availability Statement: The data presented in this study are available on request from the corresponding author.

Conflicts of Interest: The authors declare no conflict of interest.

References

1. Sun, C.; Negro, E.; Vezzù, K.; Pagot, G.; Cavinato, G.; Nale, A.; Herve, Y.; Di, V. Hybrid inorganic-organic proton-conducting membranes based on SPEEK doped with WO₃ nanoparticles for application in vanadium redox flow batteries. *Electrochim. Acta* **2019**, *309*, 311–325. [[CrossRef](#)]
2. Barbir, F. *PEM Fuel Cells: Theory and Practice*; Academic Press: Cambridge, MA, USA, 2013; ISBN 9780123877109.
3. Park, S.; Lee, J.-W.; Popov, B.N. A review of gas diffusion layer in PEM fuel cells: Materials and designs. *Int. J. Hydrog. Energy* **2012**, *37*, 5850–5865. [[CrossRef](#)]
4. Popov, B.N.; Park, S.; Lee, J.W. Effect of Gas Diffusion Layer Structure on the Performance of Polymer Electrolyte Membrane Fuel Cell. In *Electrocatalysts for Low Temperature Fuel Cells: Fundamentals and Recent Trends*; Wiley: Hoboken, NJ, USA, 2017; p. 616. ISBN 9783527803873.
5. Ijaodola, O.S.; El-Hassan, Z.; Ogungbemi, E.; Khatib, F.N.; Wilberforce, T.; Thompson, J.; Olabi, A.G. Energy efficiency improvements by investigating the water flooding management on proton exchange membrane fuel cell (PEMFC). *Energy* **2019**, *179*, 246–267. [[CrossRef](#)]
6. Majlan, E.H.; Rohendi, D.; Daud, W.R.W.; Husaini, T.; Haque, M.A. Electrode for proton exchange membrane fuel cells: A review. *Renew. Sustain. Energy Rev.* **2018**, *89*, 117–134. [[CrossRef](#)]
7. Cindrella, L.; Kannan, A.M.; Lin, J.F.; Saminathan, K.; Ho, Y.; Lin, C.W.; Wertz, J. Gas diffusion layer for proton exchange membrane fuel cells—A review. *J. Power Sources* **2009**, *194*, 146–160. [[CrossRef](#)]
8. Chen, J.; Matsuura, T.; Hori, M. Novel gas diffusion layer with water management function for PEMFC. *J. Power Sources* **2004**, *131*, 155–161. [[CrossRef](#)]
9. Peng, M.; Dong, E.; Chen, L.; Wang, Y.; Tao, W.-Q. Effects of Cathode Gas Diffusion Layer Configuration on the Performance of Open Cathode Air-Cooled Polymer Electrolyte. *Energies* **2022**, *15*, 6262. [[CrossRef](#)]
10. Kitahara, T.; Konomi, T.; Nakajima, H. Microporous layer coated gas diffusion layers for enhanced performance of polymer electrolyte fuel cells. *J. Power Sources* **2010**, *95*, 2202–2211. [[CrossRef](#)]
11. Kim, T.; Lee, S.; Park, H. A study of water transport as a function of the micro-porous layer arrangement in PEMFCs. *Int. J. Hydrog. Energy* **2010**, *35*, 8631–8643. [[CrossRef](#)]
12. Wu, R.; Liao, Q.; Zhu, X.; Wang, H. Liquid and oxygen transport through bilayer gas diffusion materials of proton exchange membrane fuel cells. *Int. J. Heat Mass Transf.* **2012**, *55*, 6363–6373. [[CrossRef](#)]
13. Chun, J.H.; Jo, D.H.; Kim, S.G.; Park, S.H.; Lee, C.H.; Kim, S.H. Improvement of the mechanical durability of micro porous layer in a proton exchange membrane fuel cell by elimination of surface cracks. *Renew. Energy* **2012**, *48*, 35–41. [[CrossRef](#)]
14. Martín-Alcántara, A.; González-Morán, L.; Pino, J.; Guerra, J. Effect of the Gas Diffusion Layer Design on the Water Management and Cell Performance of a PEM Fuel Cell. *Processes* **2022**, *10*, 1395. [[CrossRef](#)]
15. Sim, J.; Kang, M.; Min, K. Effects of basic gas diffusion layer components on PEMFC performance with capillary pressure gradient. *Int. J. Hydrog. Energy* **2021**, *46*, 27731–27748. [[CrossRef](#)]
16. Park, S.B.; Kim, S.; Park, Y.; Oh, M. Fabrication of GDL microporous layer using PVDF for PEMFCs Fabrication of GDL microporous layer using PVDF for PEMFCs. *J. Phys. Conf. Ser.* **2009**, *165*, 012046. [[CrossRef](#)]
17. Balzarotti, R.; Latorrata, S.; Stampino, P.G.; Cristiani, C.; Dotelli, G. Development and characterization of non-conventional micro-porous layers for PEM fuel cells. *Energies* **2015**, *8*, 7070–7083. [[CrossRef](#)]
18. Can, E.M.; Mufundirwa, A.; Wang, P.; Iwasaki, S.; Kitahara, T.; Nakajima, H. Superhydrophobic fluorinated carbon powders for improved water management in hydrogen fuel cells. *J. Power Sources* **2022**, *548*, 232098. [[CrossRef](#)]
19. Lee, F.C.; Ismail, M.S.; Ingham, D.B.; Hughes, K.J.; Ma, L.; Lyth, S.M.; Pourkashanian, M. Alternative architectures and materials for PEMFC gas diffusion layers: A review and outlook. *Renew. Sustain. Energy Rev.* **2022**, *166*, 112640. [[CrossRef](#)]
20. Mariani, M.; Latorrata, S.; Patrignani, S.; Gallo Stampino, P.; Dotelli, G. Characterization of novel graphene-based microporous layers for Polymer Electrolyte Membrane Fuel Cells operating under low humidity and high temperature. *Int. J. Hydrog. Energy* **2020**, *45*, 7046–7058. [[CrossRef](#)]
21. Garsany, Y.; Bancroft, C.H.; Atkinson, R.W.; Bethune, K.; Gould, B.D.; Swider-lyons, K.E. Effect of GDM Pairing on PEMFC Performance in Flow-Through and Dead-Ended Anode Mode. *Molecules* **2020**, *25*, 1469. [[CrossRef](#)]

22. Kitahara, T.; Nakajima, H. Microporous layer-coated gas diffusion layer to reduce oxygen transport resistance in a polymer electrolyte fuel cell under high humidity conditions. *Int. J. Hydrog. Energy* **2016**, *41*, 9547–9555. [[CrossRef](#)]
23. Peighambaroust, S.J.; Rowshanzamir, S.; Amjadi, M. Review of the proton exchange membranes for fuel cell applications. *Int. J. Hydrog. Energy* **2010**, *35*, 9349–9384. [[CrossRef](#)]
24. Kitahara, T.; Nakajima, H.; Okamura, K. Gas diffusion layers coated with a microporous layer containing hydrophilic carbon nanotubes for performance enhancement of polymer electrolyte fuel cells under both low and high humidity conditions. *J. Power Sources* **2015**, *283*, 115–124. [[CrossRef](#)]
25. Latorrata, S.; Stampino, P.G.; Amici, E.; Pelosato, R.; Cristiani, C.; Dotelli, G. Effect of rheology controller agent addition to Micro-Porous Layers on PEMFC performances. *Solid State Ion.* **2012**, *216*, 73–77. [[CrossRef](#)]
26. Latorrata, S.; Stampino, P.G.; Cristiani, C.; Dotelli, G. Preparation, ex situ and in situ Characterization of Gas Diffusion Media Containing and Non-Containing Carboxymethylcellulose for PEM Fuel Cells. *Fuel Cells* **2015**, *15*, 463–471. [[CrossRef](#)]
27. Tracton, A.A. *Coatings Technology: Fundamentals, Testing, and Processing Techniques*; CRC Press: Boca Raton, FL, USA, 2006; ISBN 9781420044089.
28. Latorrata, S.; Stampino, P.G.; Cristiani, C.; Dotelli, G. Development of an optimal gas diffusion medium for polymer electrolyte membrane fuel cells and assessment of its degradation mechani. *Int. J. Hydrog. Energy* **2015**, *40*, 14596–14608. [[CrossRef](#)]
29. Kitahara, T.; Nakajima, H.; Mori, K. Hydrophilic and hydrophobic double microporous layer coated gas diffusion layer for enhancing performance of polymer electrolyte fuel cells under no-humidification at the cathode. *J. Power Sources* **2012**, *199*, 29–36. [[CrossRef](#)]
30. Shrestha, P.; Banerjee, R.; Lee, J.; Ge, N.; Muirhead, D.; Liu, H.; Kai, A.; Wong, C.; Ouellette, D.; Zhao, B.; et al. Hydrophilic microporous layer coatings for polymer electrolyte membrane fuel cells operating without anode humidification. *J. Power Sources* **2018**, *402*, 468–482. [[CrossRef](#)]
31. Sun, C.; Negro, E.; Nale, A.; Pagot, G.; Vezzù, K.; Zawodzinski, T.A.; Meda, L.; Gambaro, C.; Di, V. An efficient barrier toward vanadium crossover in redox flow batteries: The bilayer [Nafion/(WO₃) x] hybrid inorganic-organic membrane. *Electrochim. Acta* **2021**, *378*, 138133. [[CrossRef](#)]
32. Latorrata, S.; Stampino, P.G.; Cristiani, C.; Dotelli, G. Performance evaluation and durability enhancement of FEP-based gas diffusion media for PEM fuel cells. *Energies* **2017**, *10*, 2063. [[CrossRef](#)]
33. Latorrata, S.; Pelosato, R.; Stampino, P.G.; Cristiani, C.; Dotelli, G. Use of electrochemical impedance spectroscopy for the evaluation of performance of PEM fuel cells based on carbon cloth gas diffusion electrodes. *J. Spectrosc.* **2018**, *3254375*, 1–13. [[CrossRef](#)]
34. Zhao, J.; Li, X. A review of polymer electrolyte membrane fuel cell durability for vehicular applications: Degradation modes and experimental techniques. *Energy Convers. Manag.* **2019**, *199*, 112022. [[CrossRef](#)]
35. Zhang, X.; Yang, Y.; Zhang, X.; Guo, L.; Liu, H. Performance Degradation of Proton Exchange Membrane Fuel Cell Caused by an Accelerated Stress Test. *Fuel Cells* **2019**, *19*, 160–168. [[CrossRef](#)]
36. Mariani, M.; Latorrata, S.; Gallo Stampino, P.; Dotelli, G. Evaluation of Graphene Nanoplatelets as a Microporous Layer Material for PEMFC: Performance and Durability Analysis. *Fuel Cells* **2019**, *19*, 685–694. [[CrossRef](#)]
37. Latorrata, S.; Sansotera, M.; Gola, M.; Stampino, P.G.; Navarrini, W.; Dotelli, G. Innovative Perfluoropolyether-Functionalized Gas Diffusion Layers with Enhanced Performance in Polymer Electrolyte Membrane Fuel Cells. *Fuel Cells* **2020**, *20*, 166–175. [[CrossRef](#)]
38. Reshетенko, T.; Ben, B.L. Electrochimica Acta Impact of a gas diffusion layer's structural and textural properties on oxygen mass transport resistance in the cathode and performance of proton exchange membrane fuel cells. *Electrochim. Acta* **2021**, *371*, 137752. [[CrossRef](#)]
39. Athanasaki, G.; Wang, Q.; Shi, X.; Chauhan, N.; Vimala, V. Design and development of gas diffusion layers with pore forming agent for proton exchange membrane fuel cells at various relative humidity conditions. *Int. J. Hydrog. Energy* **2020**, *46*, 6835–6844. [[CrossRef](#)]
40. Zahiri, B.; Felix, R.M.; Hill, A.; Kung, C.H.; Sharma, T.; Real, J.D.; Mérida, W. Applied Surface Science Through-plane wettability tuning of fibrous carbon layers via O₂ plasma treatment for enhanced water management. *Appl. Surf. Sci.* **2018**, *458*, 32–42. [[CrossRef](#)]
41. Van Nguyen, T.; Ahosseini, A.; Wang, X.; Yarlagadda, V.; Kwong, A.; Weber, A.Z.; Deevanhxay, P.; Tsushima, S. Hydrophobic Gas-Diffusion Media for Polymer-Electrolyte Fuel Cells by Direct Fluorination. *J. Electrochem. Soc.* **2015**, *162*, F1451–F1460. [[CrossRef](#)]
42. Latorrata, S.; Balzarotti, R.; Gallo Stampino, P.; Cristiani, C.; Dotelli, G.; Guilizzoni, M. Design of properties and performances of innovative gas diffusion media for polymer electrolyte membrane fuel cells. *Prog. Org. Coat.* **2015**, *78*, 517–525. [[CrossRef](#)]
43. Hui, S.; Ying, Z.; Lin, X.; Sun, J.; Wang, Y.; Fu, Q.; Li, J. Novel scalable freezing-pore-forming strategy for constructing hierarchically porous carbon materials for supercapacitors. *J. Alloy. Compd.* **2020**, *846*, 156235. [[CrossRef](#)]
44. Liu, Z.; Chen, H. A novel hydrophilic-modified gas diffusion layer for proton exchange membrane fuel cells operating in low humidification. *Int. J. Energy Res.* **2021**, *45*, 16874–16883. [[CrossRef](#)]

45. Hwan, J.; Tae, K.; Hyun, D.; Young, J.; Gon, S.; Hee, S.; Sook, E.; Jyoung, J.; Hyun, S. Development of a novel hydrophobic / hydrophilic double micro porous layer for use in a cathode gas diffusion layer in PEMFC. *Int. J. Hydrog. Energy* **2011**, *36*, 8422–8428. [[CrossRef](#)]
46. Ahn, M.; Cho, Y.; Cho, Y.; Kim, J.; Jung, N.; Sung, Y. Influence of hydrophilicity in micro-porous layer for polymer electrolyte membrane fuel cells. *Electrochim. Acta* **2011**, *56*, 2450–2457. [[CrossRef](#)]

Disclaimer/Publisher’s Note: The statements, opinions and data contained in all publications are solely those of the individual author(s) and contributor(s) and not of MDPI and/or the editor(s). MDPI and/or the editor(s) disclaim responsibility for any injury to people or property resulting from any ideas, methods, instructions or products referred to in the content.